Additive Manufacturing of Commercial Polypropylene Grades of Similar Molecular Weight and Molecular Weight Distribution

Mohamed I. Nour

Thesis submitted to the faculty of the Virginia Polytechnic Institute and State University in partial fulfillment of the requirements for the degree of

Master of Science

In

Chemical Engineering

Michael J. Bortner, Chair

Stephen M. Martin

Jacob J. Fallon

May 7, 2024

Blacksburg, VA

Keywords: Additive Manufacturing, Fused Filament Fabrication, Commercial Polypropylene, Polymer Blends, Rheology

Additive Manufacturing of Commercial Polypropylene Grades of Similar Molecular Weight and Molecular Weight Distribution

Mohamed I. Nour

ABSTRACT

Filament-based material extrusion additive manufacturing (MEAM) is an established technique in additive manufacturing (AM). However, semicrystalline polymers, such as polypropylene (PP), have limited commercial use in MEAM processes in the past due to their rapid crystallization kinetics and the subsequent effect on the integrity of the generated structures. The rapid crystallization of PP can be controlled by formulating blends of PP with hydrocarbon resins to enable longer re-entanglement times for interlayer adhesion. While the topic of formulating PP blends/composites with other materials to improve the printability has been investigated, variation in properties of commercial PP grades, of similar molecular weight (MW) and molecular weight distribution (MWD), on printability is still to be investigated. Those commercial PP grades can have wide variation in properties such as Melt Flow Index (MFI), additive content, and polymer architecture which can impact material properties relevant to printability. To investigate the effect of properties of commercial PP on their printability and mechanical performance, different commercial PP grades, with different properties, are blended with a fixed loading of hydrogenated resins, and the consequent effects on the mechanical properties of MEAM generated PP structures are studied via mechanical analysis. Tensile strength and the extent of interlayer adhesion in the 3D printed blends are characterized through rheological measurements. These measurements emphasize the importance of the relative location of the storage/loss modulus crossover point via small oscillatory frequency sweeps. We specifically show that a relatively higher crossover frequency will correlate with improved interlayer adhesion and reduced warpage in printed structures. However, this improvement is accompanied by a tradeoff, resulting in inferior tensile strength and an increased degree of print orientation anisotropy.

Additive Manufacturing of Commercial Polypropylene Grades of Similar Molecular Weight and Molecular Weight Distribution

Mohamed I. Nour

GENERAL AUDIENCE ABSTRACT

Additive Manufacturing (AM), commonly known as 3D printing, is a transformative technology with high potential to revolutionize the manufacturing landscape. Polymers are widely used in AM for various applications. As a result, extensive research is conducted to enhance the printability and properties of printed polymer structures. Polypropylene (PP) exhibits desirable mechanical, optical, and chemical properties that make its use in AM attractive. Despite this potential, optimizing the use of PP in 3D printing remains challenging. Consequently, extensive research is underway to improve the printability of PP. However, the effects of including additives to enhance the properties of commercial PP grades are often overlooked. We demonstrate that the choice of commercial PP grade is crucial to the mechanical and structural properties of structures generated via AM. This was established by developing a systematic experimental procedure to assess the printability of various PP grades and to measure their key mechanical and structural properties.

DEDICATION

To my parents and brothers.

ACKNOWLEDGEMENTS

I would like to express my profound gratitude to my advisor, Dr. Michael Bortner, for his invaluable advice and mentorship throughout my Master's journey. Joining his lab with no prior background in polymers, I was quickly able to integrate and contribute, thanks to his guidance. I am confident in saying that my growth as a researcher is largely due to Dr. Bortner's influence.

I am also thankful to my committee members, Dr. Stephen Martin and Dr. Jake Fallon, for their critical insights and guidance during the early stages of my project. Their contributions were instrumental in shaping my thesis topic.

My appreciation extends to all members of the Polymer Composite and Materials Laboratory. Their constant support and assistance were crucial in overcoming the numerous challenges encountered during my project. I am sincerely grateful for their camaraderie and collaborative spirit.

I owe a tremendous debt of gratitude to my parents. Their boundless support, wise guidance, and constant prayers have profoundly shaped my character and aspirations. The decision to pursue a graduate degree was inspired by their belief in me and their unwavering encouragement.

Lastly, and most importantly, I'm immensely grateful to God for all the blessings He has provided me throughout my life and graduate studies.

TABLE OF CONTENTS

LIST OF FIGURES

LIST OF TABLES

1 INTRODUCTION

1.1 Motivation

Additive Manufacturing (AM), commonly known as 3D printing, is a manufacturing process where material is deposited in a layer-by-layer manner to create the desired structure. Over the past few decades, AM has garnered considerable interest across industrial and academic communities over conventional manufacturing processes for its rapid prototyping capabilities, efficient material usage, and positive outlook towards contributing to sustainable manufacturing [1-3]. There are several AM techniques that have been developed over the years that are employed for various applications. As of now, AM techniques can be categorized into seven subcategories representing the breadth of manufacturing techniques it encompasses [4]. However, material extrusion additive manufacturing (MEAM) is considered the most popular and developed AM technique [5, 6]. MEAM of thermoplastic polymers, commonly known as Fused Filament Fabrication (FFF), utilizes polymer filaments that are directed through an extruder and liquefied in a heated extruder nozzle to deposit printed roads of the polymer filament in a layer-by-layer fashion to eventually establish geometries of various complexities. Those geometries are generally designed via computer aided design (CAD) [7].

Although FFF has gained widespread popularity and adoption in academia, industry, and even households, the catalogue of materials applicable for FFF is still limited [4, 8]. Currently, polylactic acid (PLA) and acrylonitrile butadiene styrene (ABS) are considered the most utilized and commercially available polymers for FFF [9, 10]. ABS was shown to have desirable properties such great mechanical properties, abrasion resistance, and chemical resistance. On the other hand, the use of PLA in FFF is desirable as it is biodegradable and resulting structures have high

geometric fidelity [4]. This dimensional accuracy of PLA prints can be attributed to the semicrystalline nature of the material. Materials with low degrees of crystallinity and slow crystallization kinetics tend to result in structures of great dimensional accuracy and insignificant warpage [7, 11]. As such, the applicability of polymeric materials in FFF is largely dependent on their inherent properties, such as their rheological and thermal properties. Extensive research in the field is ongoing to not only optimize the printing processes, but also to tune the materials' rheology and crystallization kinetics by incorporating fillers/formulating blends to establish desirable material properties and good printability.

Even though PLA is semicrystalline, polymers with higher degrees of crystallinity typically suffer when used in FFF due to poor interlayer adhesion between the layers and the subsequent warpage in the printed structure. The poor mechanical properties and structural integrity of the prints is a result of the volumetric shrinkage that results when polymers crystallize as they cool down, causing significant residual stresses. The faster the material's crystallization kinetics, the more detrimental is the effect on the mechanical and structural properties of the prints [12-14]. Consequently, the utilization of semicrystalline polymers, like polypropylene (PP), in FFF has been largely limited due to their intrinsic properties. However, employing polymers that are highly crystalline in AM is of great interest as they tend to generate structures that are mechanically superior to amorphous polymers [7]. In particular, PP is one of the world's most used polymers for various applications due to its great chemical and mechanical properties, potential for recyclability, and its competitive cost compared to other polymers [15]. As a result, extensive research has been conducted to improve the printability of PP when employed in FFF. One of the common approaches taken by researchers to improve the printability of PP is to optimize the printing process and parameters to improve the bed adhesion and reduce warpage [7, 9, 15]. Another common

approach is to incorporate fillers or formulate blends of PP with other materials to slow down the crystallization kinetics of PP and improve interlayer adhesion between the printed layers [12, 13, 16].

While optimizing the printability of PP via the incorporation of fillers/blends is promising, consideration of variation in rheological and thermal properties between commercial PP grades is of extreme importance but understudied. In general, commercially sourced PP grades tend to have differing amounts/compositions of additives in order to modify the thermal, mechanical or optical properties for different applications. In addition, PP grades manufactured from the same manufacturer could have differences in topology/ branching that might not be detected via Gel Permeation Chromatography (GPC)/ Size Exclusion Chromatography (SEC) analysis. Such differences can result in significant variations in rheological properties and crystallization kinetics of varying PP grades that will ultimately impact the printability and mechanical properties of those commercial PP grades.

1.2 Research Question and Objectives

The goal of this research is to elucidate the effect of additive packages and molecular architecture on the printability of commercial PP grades of similar molecular weight (MW) and molecular weight distribution (MWD). We aim to elucidate how different commercial PP grades of similar MW and MWD print and mechanically behave when blended with hydrocarbon resins at fixed compositions and printing parameters. By establishing the impact of additive inclusion and molecular architecture towards printability of PP, the following objective can be met:

Rheological measurements probing the relative timescales of the onset of flow regime of commercial PP grades using small amplitude oscillatory frequency sweeps (SAOS) allow

for better material selection and design for FFF by predicting: 1) the relative extent of polymer chains interlayer diffusion and mechanical anisotropy, 2) the relative mechanical strength, and 3) the relative warpage a printed PP blend might exhibit when using the same printing parameters.

Hypothesis Statement:

The crossover point of the elastic and viscous moduli, as measured using SAOS, serves as an indicator for evaluating the impact of additive packages and molecular architecture of commercial PP grades of similar MW and MWD in FFF.

In answering the above hypothesis, we predict that a relatively higher crossover frequency will correlate with improved interlayer adhesion and reduced warpage in printed structures. However, this improvement is accompanied by a tradeoff, resulting in inferior tensile strength and an increased degree of print orientation anisotropy.

Chapters 3 to 5 of this thesis are prepared as part of a manuscript in collaboration with Dr. Amy Peterson at UMass Lowell. Dr. Peterson's group will specifically focus on crystallization kinetics studies to complement the findings presented in this thesis.

2 BACKGROUND AND LITERATURE REVIEW

2.1 Additive Manufacturing

The adoption of AM, formerly known as rapid prototyping, can be dated to the late 1980s when 3D Systems launched their first AM system in 1987 based on the principles of stereolithography [17]. Since then, several AM techniques have been developed due to the potential of AM techniques in changing the manufacturing landscape. There are two main benefits that AM provides to their users [18]. The first is AM's ability to create and increase the complexity of manufactured parts with minimal effects on costs and time. The second important advantage is that AM can optimize the manufacturing process by reducing the costs entailed in conventional processes that arise from the high labor costs and the initial capital required for prototyping of new products.

Nowadays, AM can employ several materials such as metals [19, 20], ceramics [21], polymers [22], and their respective composites and blends. As such, AM products can find use in several applications that encompass industries ranging from high performance applications in automotive and biomedical sectors, to commodity products and packing in conventional manufacturing industries [3, 23].

All AM technologies share the same four components required to generate a product [19]. An AM technique requires a digital model of the part that needs to be manufactured, a material to be used to manufacture the part, a tool that lays the said material in a layer to generate a 3D structure, and a digital control system to modify/optimize the tool's manufacturing process. Due to the high variance in AM technologies, ASTM has grouped AM techniques into seven categories: binder jetting (BJ), directed energy deposition (DED), material extrusion additive manufacturing

(MEAM), material jetting (MJ), powder bed fusion (PBF), sheet lamination (SL), and VAT photopolymerization (VP) [19].

2.2 MEAM of Polymers

As mentioned earlier, MEAM, is considered the most widely used AM technique. A typical filament based MEAM process (FFF) is shown in figure 1 below [24]. Polymer filament from a spool is fed through a feeding mechanism, typically a gear drive, to enter an extrusion head. The filament is then liquified inside the extrusion head via a heating element and the liquified polymer is then pushed due to pressure applied by the plunger acting filament through a nozzle to have roads of filaments deposited in a layer-by-layer fashion on a build bed to generate a printed part.

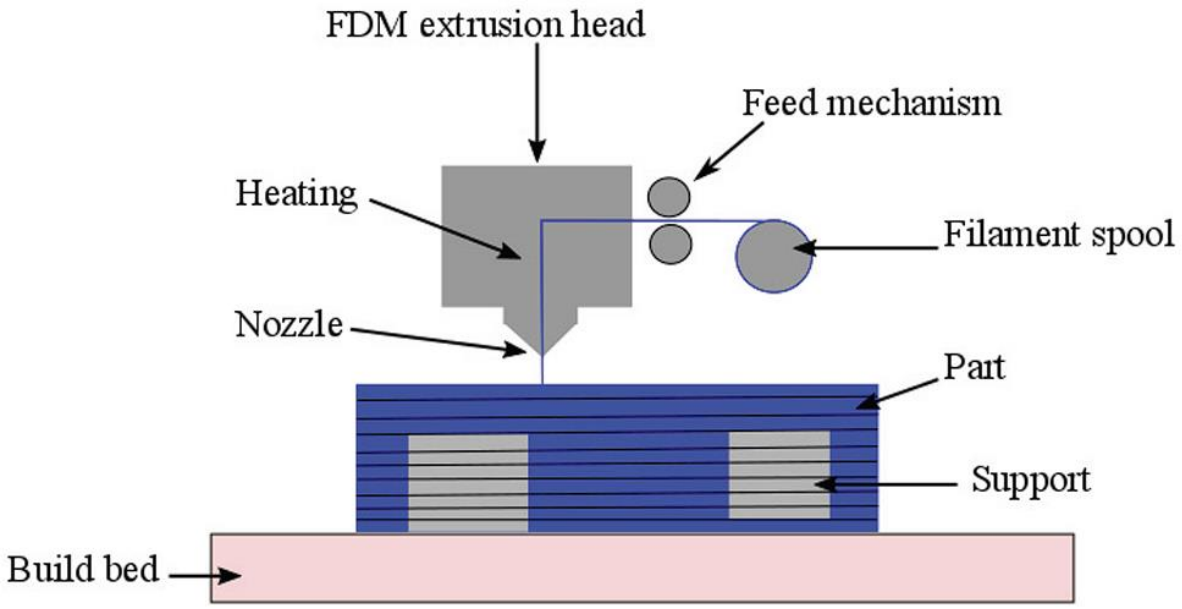

Figure 1. A typical schematic of a MEAM process. Reprinted with permission from ref [24]. Copyright 2017 Elsevier

2.2.1 Advantages and Disadvantages of FFF

There are several advantages to using FFF when compared to other AM techniques. The most apparent one is the commercial widespread use of FFF technologies. This demand by itself warrants manufacturers to continuously improve their offerings by making better printers or developing better materials for FFF applications. As a result, FFF is relatively inexpensive compared to other AM technologies. Although the cost and availability are important advantages, what potentially resulted in those advantages are the ease of scalability FFF offers in addition to its ability to build fully functional parts [19].

However, FFF comes with its own set of drawbacks. Often times, the prints experience high degrees of vertical anisotropy and inexpensive printers are unable to generate extremely fine details which could result in step structured surfaces [19]. Furthermore, the FFF process has a high degree of freedom due to the several process parameters that can be modified in order to optimize the print's mechanical and aesthetic qualities. Qattawi et. al showed that the layer height, building direction, and extrusion temperature are of high importance to the mechanical properties and structural accuracy of the final printed part [24]. The interactions between the process parameters of the FFF process, the material properties, and the control parameters have been widely studied in the literature [5, 25]. As a result of the high number of variables involved in FFF processes, the process of generating good prints involves a demanding trial and error procedure to optimize all the parameters involved in the process based on empirical data. Thus, FFF optimization is often time consuming.

2.2.2 Common Failure Modes in FFF

There are generally three common causes of failure in the FFF process that occur inside the nozzle of a MEAM machine which could result in failure of the prints or undesirable inconsistencies. Those are inconsistent filament diameter, annular backflow and filament buckling [26]. As of today, most of the FFF printers compute the amount of polymer flow needed through the nozzle based on the average diameter of filaments. If inconsistencies are severe in the filament diameter, this will reflect poorly on the printed parts via either over extrusion or under extrusion of polymer resulting in poor prints. Furthermore, as the flow of the filament is controlled by the feed mechanism shown in Figure 1, the consistency in the filament diameter and the material properties become important. If the polymer filament is too flexible, it might not be able to withstand the pressure from the feed mechanism resulting in filament buckling inside the extruder [23]. Additionally, if the shear thinning profile of the polymer is not steep enough and the filament diameter is not in agreement with the printer's specifications, then annular backflow could result in the nozzle. Hence, the rheological and thermal properties of polymers are important for MEAM and that results in limiting the catalogue of material available [23].

2.2.3 Semicrystalline Polymers in MEAM

While PLA and ABS are the most used materials in FFF, materials with better mechanical properties are desired for high performance applications. As a result, semicrystalline polymers are more desirable for these FFF applications due to their superior mechanical properties [7]. However, prints employing semicrystalline polymers tend to suffer from severe warpage due to the volume shrinkage and high residual stresses that occur due to crystallization of the polymer chains [7, 9].

In general, all AM modalities tend to generate parts that are the weakest at the interface of the adjacent layers due to chain interlayer diffusion limitations. This results in inferior mechanical properties for the prints when compared to traditional manufacturing processes such as injection molding. Semicrystalline polymers generate even weaker prints than amorphous polymers as interlayer diffusion is further limited with brief window the polymer chains have to diffuse before they crystallize. Boiko et al. showed that the healing of interphases of two semicrystalline polymers is poor as a result of the crystals inhibiting the polymer chains diffusion into the other layer [27]. Hence, they found that the bond strength between two semicrystalline layers is much weaker than that between two amorphous layers. However, welding between semicrystalline layers can be enhanced via the co-crystallization mechanism as the chains crystallize at the interface generating a strong weld [28]. Thus, by controlling the crystallization kinetics of semicrystalline polymers to extend the time frame the polymer chains have for interlayer diffusion, superior mechanical properties can be achieved in semicrystalline MEAM parts compared to parts made from amorphous polymers.

2.3 Polypropylene (PP)

PP is a semicrystalline thermoplastic that is made from propylene monomer units traditionally obtained from petroleum products. The first successful catalytic synthesis of isotactic polypropylene (iPP, henceforth simply referred to as PP) can be dated back to 1954 when the Zeigler catalyst was synthesized [29]. Despite its relatively old age as a polymer, the demand and market for PP has been continuously growing. iPP holds the second largest market share of all polymers. In 2015, the market of PP was estimated to be around 60 million tons and this is expected to grow to 120 million tons by 2030 [29]. Such tremendous growth is owed to the excellent mechanical, thermal, and physical properties of PP [30]. In fact, PP has found use in various

industrial sectors, ranging from day to day community products, to high performance parts in the automotive industry, or even medical parts [30]. Those excellent properties led researchers and industrial companies to not only use PP as a neat feedstock for their products, but also formulate blends, composites, and copolymers that are based on PP. In addition, nowadays the technology of producing PP has advanced to be able synthesize PP of high tacticity to make iPP but also synthesize a range of PP products with varying tacticity that could go all the way to syndiotactic PP (sPP) [29, 30].

As a result, researchers have found that PP has massive potential in AM as the polymer is readily available in the market, has desirable properties, and is inexpensive. Jagenteufel et al. [31] were some of the first researchers who recognized the potential of PP in AM. They showed that compared to ABS, PP is more stable at high extrusion temperatures, and has a higher melt stiffness which makes it more suitable for extrusion in MEAM. However, given the semicrystalline nature of PP, the polymer fails to produce prints of high structural qualities and good mechanical properties due to warpage from high residual stresses, and poor interlayer adhesion due to the crystals inhibiting chain interdiffusion between the printed layers. Figure 2 below shows the warpage that is commonly present in PP prints as a result of the residual stresses causing a force to lift the PP layers off the print surfaces. Nevertheless, extensive work in the field has been done to enhance the printability of PP. By disturbing the regular arrangement of PP to form random arrangement of chains, the warpage of PP parts can in theory be eliminated [13].

Two approaches have been researched in the literature to enhance the FFF of PP. The first is to optimize the parameters of the MEAM process to reduce warpage and enhance interlayer adhesion. The second is modify the material properties by incorporating fillers into PP or blending PP with other materials.

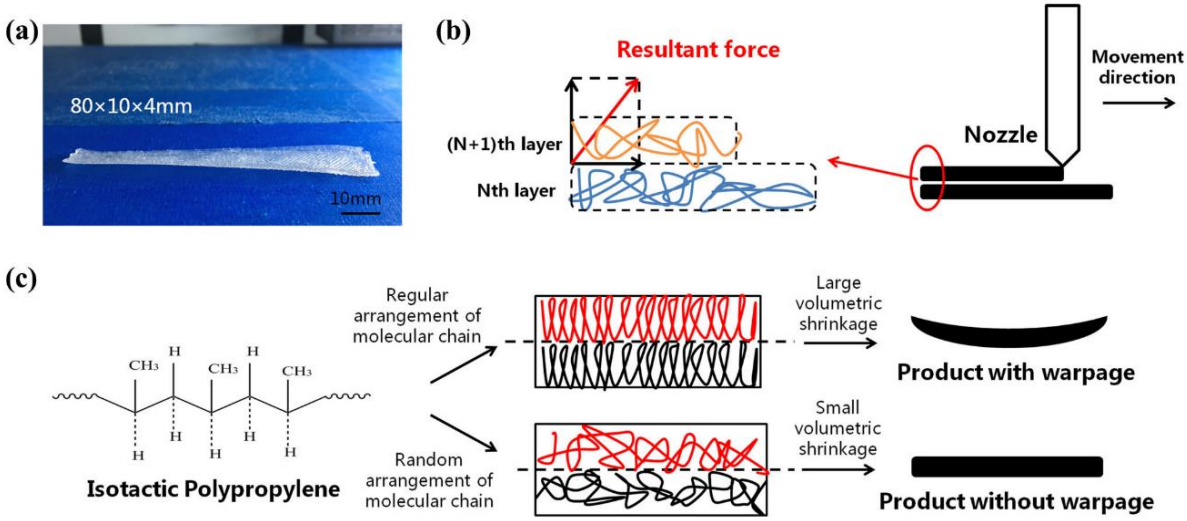

Figure 2. Warpage of pure PP in MEAM process, (b) schematic diagram of warpage generated in MEAM process, (c) schematic diagram of the relationship between warpage and the arrangement of molecular chains. Reprinted with permission from ref [13]. Copyright 2019 Springer Nature

2.3.1 Enhancing FFF of PP: Process Optimization

The research available in the literature on FFF of neat PP is limited. Much of the work on enhancing the printability of PP is focused on material optimization. Nonetheless, strides have been made in the field to understand how printability of neat PP can be generally improved in MEAM via process parameters optimization. Researchers observed that PP does not generally adhere well to the printer build platform. Spoerk et al. [15] investigated the effect of build platform material, extrusion temperature, bed temperature, and layer height on the adhesion of PP composites based materials on the printer bed. They found after a thorough parametric study that an ultra-high-molecular-weight polyethylene material is the most suitable material for the build platform. This material allows PP to adhere well to the platform without welding. As a result, the detachment of the printed part is easily achieved at room temperature without damage to printed part. In addition, they found that increasing the surface roughness of the build platform results in

better wetting between PP and platform; hence, better adhesion. They also found that by increasing the extrusion temperature and the platform temperature, and reducing the layer height, the first layer's adhesion to the platform improves.

Similarly, Bachar et al. [9] investigated the printability of neat PP with FFF. They reduced the warpage of neat PP printed parts by improving the adhesion of the first printed layer on the surface by applying a polyvinyl acetate-based glue on the surface and by adding brims on the printed part. Furthermore, they noticed that the warpage is minimized in the printed parts by reducing the infill %. However, they did not find a direct correlation between the warpage and the print height.

Some studies suggest that printing PP parts at high extrusion temperatures is beneficial. However, Wang and Gardner [32] examined the impact strength of PP parts printed at various extrusion and bed temperatures, comparing them with injection molded PP. They discovered that parts printed at a lower extrusion temperature of 200 °C exhibited higher Izod impact strength than those printed at 250 °C. While better interlayer adhesion and chain interdiffusion were observed at 250 °C, the formation of more β crystals at 200 °C contributed to the enhanced impact strength, aligning closely with that of injection molded parts. Notably, the injection molded parts contained only α crystals, whereas the printed parts featured both α and β crystals, demonstrating the influence of MEAM on PP morphology. Furthermore, they noted that a lower layer height improved interlayer chain diffusion, consistent with other findings in the literature.

The print geometry was found to have an impact on the warpage of PP parts. Hämäläinen [33] found that the degree of warpage of PP is influenced by the geometrical shape of the part printed. Parts that had sharp corners like cubes resulted in significant warpage due to the concentration of residual stresses in certain areas of the printed parts. However, cylindrical parts

resulted in less severe warpage. As a result, while optimization of the printability of PP in FFF is possible via modifications to the process parameters, the improvements from such modifications do not completely eliminate warpage or significantly enhance interlayer adhesion due to the semicrystalline nature of PP. Modifications to the part geometry and size only results in limiting the applicability of PP in FFF. As such, the solution to enhance the adoption of PP in FFF will be via a combination of both process parameter optimization and material optimization [11].

2.3.2 Enhancing FFF of PP: Material Optimization

Most of the work done on improving the printability of PP is done through modifications to the material properties. The general aim of researchers is to reduce the crystallinity of PP and extend its chains' re-entanglement window by slowing down the crystallization kinetics to enhance the printability but also ensure to maintain or enhance the inherent mechanical properties of PP. This is mostly done by incorporating fillers or blending PP with other materials to formulate blends. By doing so, the ordered regular arrangement that PP chains usually exhibit is disrupted as shown in Figure 2. There are various materials that have been explored in the literature as potential fillers in PP systems and their underlying effect on mechanical properties, warpage, etc. A few of them are cellulose nanofibrils, short glass fibers, carbon fibers, glass spheres and many more [11].

For example, Spoerk et al [34] showed that PP systems filled with 30 vol% of aminosilane-coated borosilicate glass spheres reduce the warpage associated with neat PP prints but also improve the mechanical properties such as the tensile strength and toughness to be comparable to injection molded PP tensile results. They note that the use of compatibilizers is important when using glass spheres as fillers in order maintain the mechanical properties of the prints. Another approach to enhance the printability of PP is by blending it with other materials. Peng et al [13] utilized nylon 6 at 30 wt% loading to enhance the mechanical properties of PP blends with the help

of a compatibilizer to reduce warpage. The blend that they formulated resulted in the disruption of ordered PP chains and this resulted in better chain interdiffusion between the layers.

Hydrocarbon resins have been well documented to reduce crystallinity and modify the crystallization kinetics and morphology of PP [35, 36]. The use of low MW hydrocarbon resins to enhance the mechanical properties and structural accuracy of PP prints was recently explored by Das et al. [16]. The authors explored the use of both partially and fully hydrogenated hydrocarbon resins to formulate blends with PP at different loading levels. They found that by increasing the loading levels of the hydrocarbon resins, the warpage and mechanical properties of printed parts significantly improved as a result of reducing the crystallinity and slowing down the crystallization kinetics and the formation of a two-phase morphology at 20% loadings.

While there is an abundance of materials that could be incorporated with PP to enhance the printability and mechanical performance of the prints, PP grades that are commercially sourced often times have variation in their MW and thermal properties. As such, a thorough understanding of those properties is needed for better material design. A recent study by Baouch et al [37] explored the effect of MW and crystallization kinetics of neat PP in MEAM. They found that there is a flow-enhanced crystallization phenomenon that occurs to PP during the MEAM process. Consequently, this has an impact on the welding process at the layers' interface which weakens the interlayer bonding. This effect is more apparent as the MW of PP increases. On the other hand, the weld strength increases as the crystallization time becomes longer.

The variables that need to be assessed when dealing with commercial PP products become more difficult to isolate. Aside from differences in the MW, there can be differences in the MWD, additive packages incorporated by the manufacturer to modify the properties of PP, and molecular architecture of PP based on the tacticity level and topology. A general characterization technique needs to be established to support the selection of PP grades based on easily measurable design parameters.

3 MATERIALS AND METHODS

This chapter provides a detailed overview of the materials used in this study, including their specifications and sourcing. We will also explore the methods employed for compounding and processing these materials. Furthermore, this section outlines the rheological, thermal, and mechanical measurements that form the basis for the analyses presented in Chapter 4.

3.1 Materials

Three commercially available polypropylene homopolymer grades of similar MW and MWD were obtained from Braskem America, Inc. Table 1 below lists the number average MW (M_n, g mol^{-1}), the weight average MW (M_w, g mol^{-1}), the polydispersity index (PDI), and the melt flow index (MFI, g $(10min)^{-1}$) for the three grades. The glass transition temperature (T_g) of those grades lies between -25 and 0 °C.

Table 1. Properties of commercial PP grades used in study

Material	Mn (g/mol)	Mw (g/mol)	PDI	MFI (g/10min)
PP1	70k	299k	4.27	3.6
PP2	78k	292k	3.74	12
PP3	70k	293k	4.18	20

A partially hydrogenated hydrocarbon resin (denoted HR), Arkon M-100, was obtained from Arakawa Chemical Industries. The degree of hydrogenation of this material is 50-60% and it has a T_g of 45 °C. and an M_n of 810 g mol^{-1}.

3.2 Thermogravimetric Analysis (TGA)

Isothermal mass loss studies were performed in a TGA5500 (TA Instruments, USA) on HR samples of 8 -12 mg to investigate the thermal stability of the material at 180, 190, and 200 °C in air and nitrogen atmospheres.

3.3 Formulation of PP/HR blends

A CW Brabender Prep-Center with an internal mixing head was used to compound blends of PP:HR in an 80:20 wt% ratio. The blended material will be denoted as PP#B, where # denotes the number designation of the commercial PP grade shown in Table 1. For example, the blend consisting of PP1 and HR will be termed PP1B. Thus, three grades of blends are formulated. The material was mixed at 190 °C for 10 min by 2 rotating blades at a constant mixing speed of 32 rpm. 45 g batches were formulated at a time due to the maximum capacity of the mixer. After the mixing period concluded for each batch, the mixer was disassembled, and the blended material was collected. Samples collected were processed in a grinder to generate small sized pellets for further processing into filament form.

3.4 Differential Scanning Calorimetry (DSC)

Samples of 10-15 mg mass were each contained inside TA Instruments Tzero pans and tested using a Q2000 Series TA instruments differential scanning calorimeter. A nitrogen purge flow of 50 mL min^{-1} was maintained as samples went through a non-isothermal heat-cool-heat cycle from 50 – 190 °C. The heating rate was set to 10 °C min^{-1}, while the cooling rate was set to 5 °C min^{-1}.

The % crystallinity of the tested samples were calculated based on the following equation accounting for the HR content in the blends:

$$\%\ crystallinity = \frac{H_M}{H_M^{\circ}(1 - w_{HR})} \times 100\% \qquad (1)$$

where H_M is the enthalpy of melting of the sample obtained from the second heating cycle, H_M° is the enthalpy of melting of a 100% crystalline PP and is found to be 207.1 J g^{-1} [38], and w_{HR} is the weight fraction of HR in the blended samples.

3.5 Rheological Charecterization of Neat PP and Blends

Samples of neat PP and blends were each pressed, at 200 °C under an applied pressure of 1.9 GPa, using a Carver press (Carver Inc., USA) to obtain compression molded discs that are 25 mm in diameter and 1 mm in thickness. Small angle oscillatory sweeps (SAOS) (0.1 - 623 s^{-1}) were performed using a TA Instruments AR-G2 rheometer with a 25 mm diameter cone and plate fixture of an angle of 0.102 radians and a gap of 0.540 mm. The tests were performed at 180 °C for both the neat PP and blends to capture characteristic timescales of the samples. In addition, the blends were also tested at 200 °C which is the MEAM printing temperature.

3.6 Filament Generation

The pellets of the blends were extruded using a Filabot EX2 single screw extruder at 180 °C. The extrusion speed was set to 18 rpm and monitored to generate filaments with a diameter of 1.70 ± 0.1 mm that is suitable for MEAM. The extruded filament was cooled using a water bath. The filament diameter was measured online using a Filabot filament spooler equipped with a Mitutoyo caliper.

3.7 FFF of Blends

A Prusa MK3S+ printer equipped with a 0.4 mm nozzle was used to print ASTM Type V tensile bars using the filaments made from the blends. The printer's nozzle temperature was set to 200 °C and the bed temperature was set to 115 °C. Painter tape was placed on the printer bed surface and glue was applied on it to enhance bed surface adhesion with the printed parts. The infill of the prints was set to be 100% and the printing speed was maintained at 20 mm s^{-1}. The extrusion with and height were set to be 0.35 mm and 0.30 mm, respectively. The printer's cooling fan was turned off to not enhance the cooling rate of the polymer. Two print orientations were

investigated i.e. 0° and 90° raster angles prints. For each blend, at least five tensile parts were printed for each of the print orientations.

3.8 Injection Molding of Neat PP

A Boy 35E injection molding machine was used to produce dog-bone tensile bars from the neat PP grades. The barrel temperature was set at 200 °C and the mold temperature was 60 °C. The infill pressure was set to 120 bar and the hold pressure was set to 110 bar. The dog-bone tensile bars were collected after running the process five times, generating 20 parts per grade. The samples were collected in a water bath and subsequently dried in a vacuum oven at 60 °C before running the tensile tests. The tensile bars have a gauge length of 12.5 mm, width of 3.30 mm and a thickness of 1.55 mm.

3.9 Tensile Testing of Printed and Injection Molded Parts

All tensile properties of the printed blends parts and neat PP injection molded parts were measured by an Instron mechanical tester (Model 4204) with a 2 kN load cell at room temperature (~22 °C). The crosshead speed was maintained at 10 mm/min. The tensile properties of each material were calculated by the average properties of at least five samples.

4 RESULTS AND DISCUSSION

4.1 Isothermal Stability of the Hydrocarbon Resin

To select the processing temperatures throughout this study, thermal stability studies are required to be performed on HR. As the time duration of the several processing steps employed in this study vary in duration, it is important to assess the thermal stability under isothermal conditions to appropriately select the operating temperatures for each step. Thus, isothermal TGA tests were performed at several temperatures of interest under both air and nitrogen media. Figure 3 shows the results of the TGA tests conducted on HR at 180 °C, 190 °C, 200 °C.

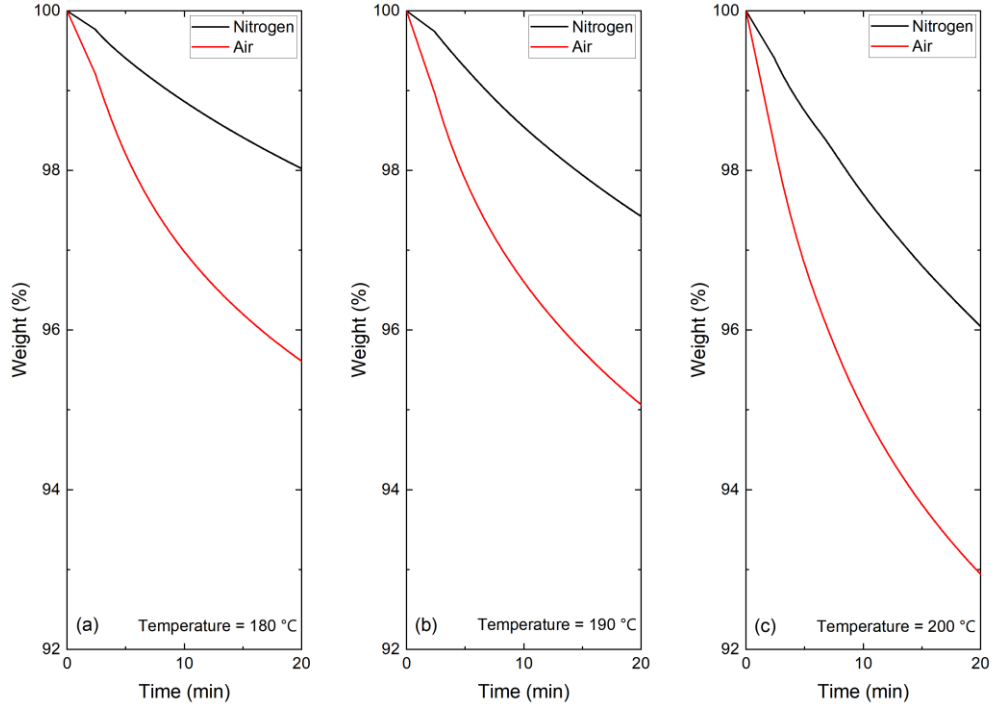

Figure 3. TGA tests on HR under air and nitrogen media at (a) 180 °C, (b) 190 °C, and (c) 200 °C

Das et al. previously reported that HR undergoes a 5 wt% degradation at 216 °C when TGA is conducted under non-isothermal conditions and at a heating rate of 10 °C min^{-1} [16]. Accordingly, any processing steps should be limited to 200 °C to minimize the loss of material.

Figure 3 shows that as the isothermal temperature setpoint increases, the extent of degradation increases under both air and nitrogen purge. Under an air atmosphere, the extent of degradation is greater than when under nitrogen due to oxidative thermal degradation effects. The blend compounding using the Brabender mixer has the longest processing time of 10 min. At the 10 min mark, the degradation of HR at 180 °C, 190 °C, and 200 °C results in wt% loss of 3%, 3.4%, and 5%, respectively. While the actual degradation during the mixing process is expected to be higher due to shear effects, the thermal stability at 10 min is approximately similar at the three temperatures. As a result, 190 °C was set as the blend formulation temperature given the relatively similar thermal stability of HR with consideration to the viscosity of PP at the given temperature.

Since during the printing process, HR has a low residence time in the extruder nozzle, the extruder temperature was set at the upper limit of 200 °C to enhance printability by lowering the viscosity of the blends during the extrusion process.

4.2 Melting, Crystallization, and Crystallinity of Neat PP and Blends

4.2.1 Investigation of Melting, Crystallization, and Crystallinity of Neat PP Samples

As the crystallinity and crystallizablility of polymers affect their printability and successful utilization in FFF, it is important to investigate the melting, crystallization, and crystallinity of the commercial PP grades that are being studied. Figure 4 shows the melting endotherms and cooling exotherms for the three PP grades. While the MW and MWD distribution of those grades are similar as shown in Table 1, commercial PP grades tend to have differences in their additive packages and molecular architecture to tune the properties of the materials to their desired applications. Yanjie et al. [39] showed that different nucleating agents added to PP can significantly

affect the morphology crystallization kinetics of PP. As a result, one can expect that with such modifications of the base polymer's behavior, differences in printability can arise.

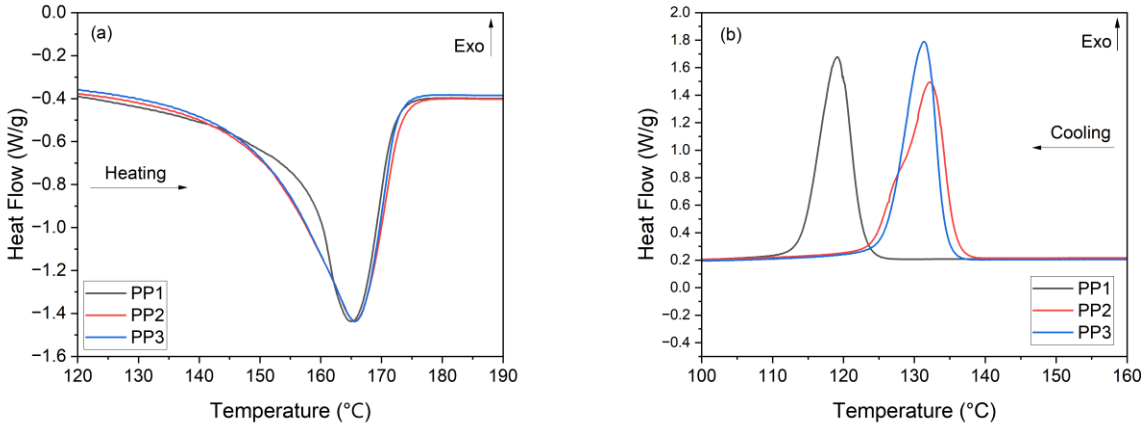

Figure 4. (a) 2nd DSC melting endotherm from the non-isothermal heat-cool-heat cycle for the different commercial PP grades, (b) DSC cooling exotherm from the non-isothermal heat-cool-heat cycle for the different commercial PP grades

Table 2 tabulates the relevant data extracted from Figure 4. The peak melting temperatures for the three PP grades are extremely similar around ~ 165.5 °C . However, we can see differences in the peak crystallization temperatures. There is a considerable difference in the peak crystallization temperature of PP1 (119.1 °C), compared to that of PP2 (132.2 °C) and PP3 (131.4°C). Such differences can be expected due to the differences in additive packages, incorporated by the manufacturer, and molecular architecture PP which most likely affect the morphology and crystallography of the different grades. Furthermore, the similarity between the peak crystallization temperatures of PP2 and PP3 does not come as a surprise. It is important to note that while all those three PP grades are sourced from the same manufacturer, PP2 and PP3 are from the same family of PP products. As such, one could expect that differences in the additive packages and molecular architecture might not be as drastic between those two grades when they are compared to PP1. On the other hand, we see that the % crystallinity for all the three grades,

determined by equation (1), is quite similar and lies around 52%. Therefore, any differences in printability of those grades will likely be due to differences in crystallization kinetics and rheology.

Table 2. Peak melting and cooling temperatures, and enthalpies of melting and crystallization from non-isothermal DSC data of neat PP grades. % crystallinity is calculated from equation (1)

Material	Peak melting temperature (°C)	Enthalpy of melting (J g^{-1})	Peak crystallization temperature (°C)	Enthalpy of crystallization (J g^{-1})	Crystallinity (%)
PP1	165.03	107.7	119.08	108	52.0
PP2	165.53	106.4	132.18	105.7	51.4
PP3	165.51	108.7	131.41	107.8	52.5

4.2.2 Effect of HR on Melting, Crystallization, and Crystallinity of PP in Blends

As this work will primarily focus on printing the blends of the respective PP grades with HR at 80:20 wt% ratio, it is important to investigate the effect of HR on the melting, crystallization, and crystallinity of PP in those blends. Figure 5 shows the effect of HR on the heating endotherms and cooling exotherms of PP in those blends. We can see a general trend of shifting the melting and crystallization peak temperatures to lower values of 117.0 °C, 119.5 °C, and 121.2 °C for PP1B, PP2B, and PP3B, respectively. This shift can be attributed to disturbance of the crystallizability of PP. Table 3 tabulates the DSC results from Figure 5. The peak melting temperatures of all the blends reduced to a similar temperature of ~160 °C. In addition, as expected, the % crystallinity of PP normalized with HR content has reduced for all the three blends to a similar extent. The reduction in crystallinity of PP due to the incorporation of HR in the blends range between 1.4 % to 6.3%. Such results are in line with previous studies that compound PP with hydrocarbon resins [16, 40].

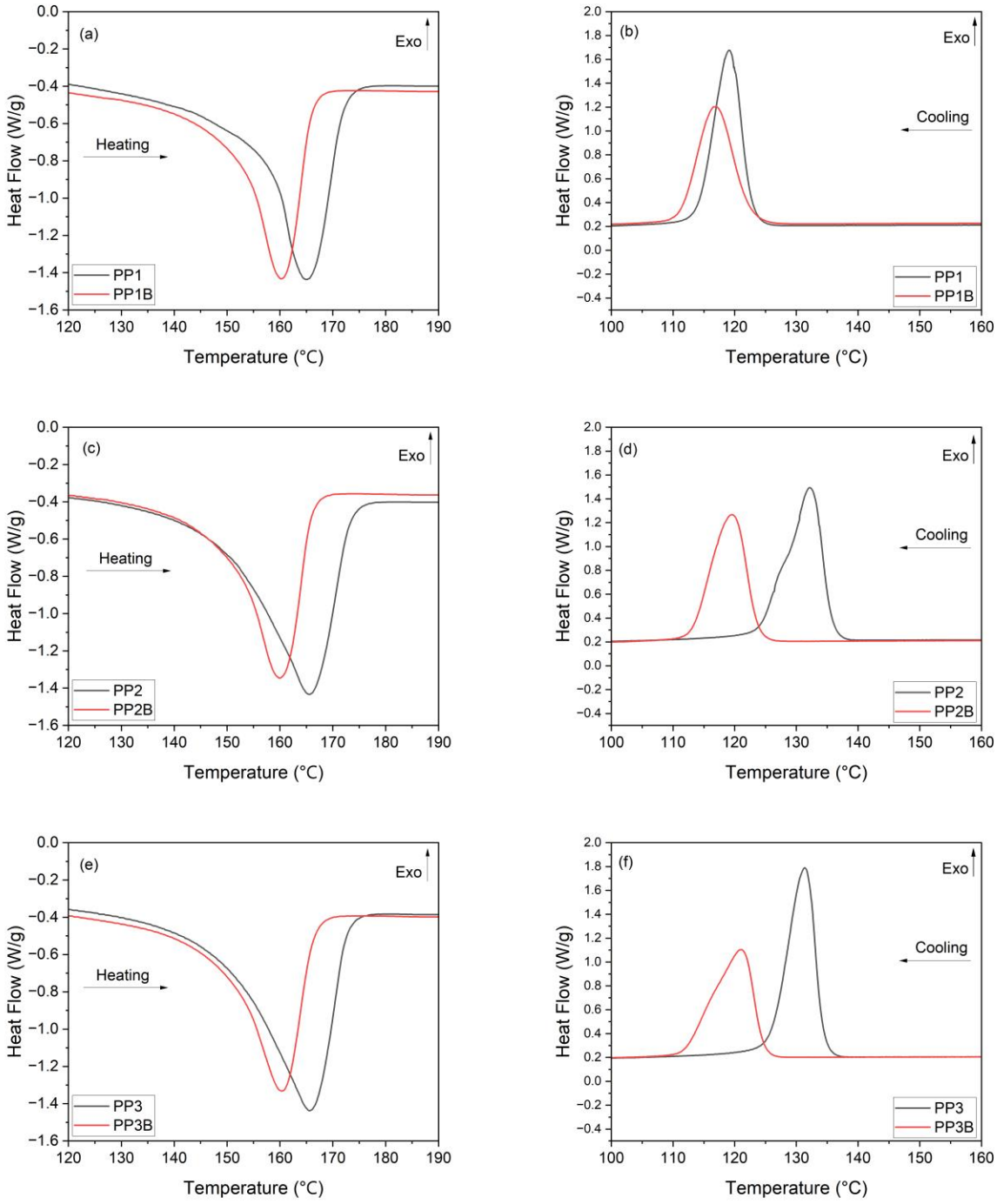

Figure 5. DSC (a) 2nd melting endotherm and (b) cooling exotherm from the non-isothermal heat-cool-heat cycle for the PP1 and PP1B, (c) 2nd melting endotherm and (d) cooling exotherm from the non-isothermal heat-cool-heat cycle for the PP2 and PP2B, (e) 2nd melting endotherm and (f) cooling exotherm from the non-isothermal heat-cool-heat cycle for the PP3 and PP3B

Notably, the peak crystallization temperatures for all the blends are similar. However, the shift in peak crystallization temperature between PP1B and PP1 is not as significant as the shifts observed between PP2B and PP2, and PP3B and PP3. Specifically, PP3B shows a drop of only 1.7% from the peak crystallization temperature of PP1, while the drops observed in PP2B and PP3B are 9.6% and 7.8%, respectively. Such differences indicate that HR affects the thermal properties of these commercial PP grades differently. This underscores the importance of recognizing property variations among PP grades, particularly across different product families. Future studies focusing on crystallization kinetics, crystallite type, and morphology will further elucidate the impact of HR on thermal properties.

Table 3. Peak melting and cooling temperatures, and enthalpies of melting and crystallization from non-isothermal DSC data of blends. % crystallinity is calculated from equation (1)

Material	Peak melting temperature (°C)	Enthalpy of melting (J g^{-1})	Peak crystallization temperature (°C)	Enthalpy of crystallization (J g^{-1})	Crystallinity (%)
PP1B	160.1	86.0	117.0	85.1	50.7
PP2B	160.0	86.1	119.5	86.9	50.7
PP3B	160.2	83.6	121.2	84.0	49.2

4.3 Rheology of Neat PP and Blends

4.3.1 Effect of Additives and Topology on the Low Frequency Crossover Points of Neat PP Grades

Rheological characterization of polymers can provide insight into the printability of said polymers during MEAM. SAOS rheological measurements were performed on the neat PP grades to study the behavior of the storage modulus (G') and loss modulus (G'') as a function of frequency. The change of G' and G'' with frequency provides us with an indication of the polymer behavior at the small length scales. Typically, thermoplastic polymers undergo three stage

transitions depending on the conditions applied to them. They can either be in a glassy state, a rubbery plateau region, or in a flow regime. The crossover of G' and G'' at low frequency values determines the transition between the flow regime and the rubbery plateau. For polymers that exhibit entangled polymer dynamics, such as PP, the crossover frequency signifies an important relaxation time known as the reptation time τ_{rep}. The τ_{rep} is the time a polymer chain in the melt takes to diffuse along the contour of it tube, indicating beginning of polymer flow. This characteristic time has a direct correlation with the viscosity and MW of the polymer [41]. Figure 6 captures the crossover points between G' and G'' for the three PP grades through SAOS measurements at 180 °C.

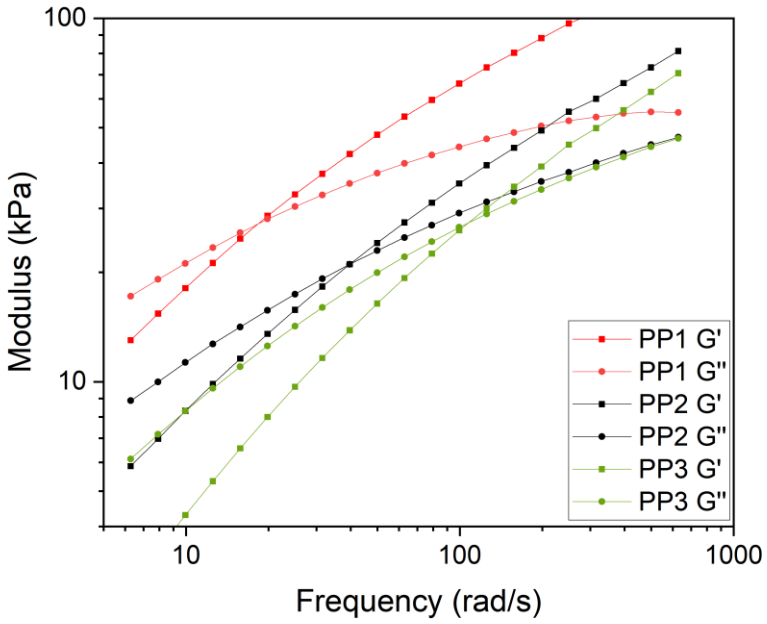

Figure 6. SAOS at 180 °C showing the crossover points between G' and G'' curves of the different PP grades

Generally, the MFI of a polymer is considered an indirect measure of MW; the higher the MFI, the lower the MW. Variations in MW and MWD in polymers are known to affect the crossover point location, as illustrated in Figure 7. The MW influences the horizontal position (frequency), while MWD impacts the vertical position (modulus), assuming all other factors remain constant [42]. A higher MW results in more entanglements within the polymer chains, increasing the τ_{rep} required for the chains to diffuse along the contours of their tubes. Conversely, a narrower MWD leads to a higher crossover modulus, due to a more limited distribution in chain mobility. However, in our study, the MW and MWD are consistent across the three PP grades studied; the variations arise from the different additive packages incorporated by the manufacturer and the differences in the molecular architecture of the PP. These differences have resulted in variations in rheological behavior similar to those typically seen with changes in MW and MWD.

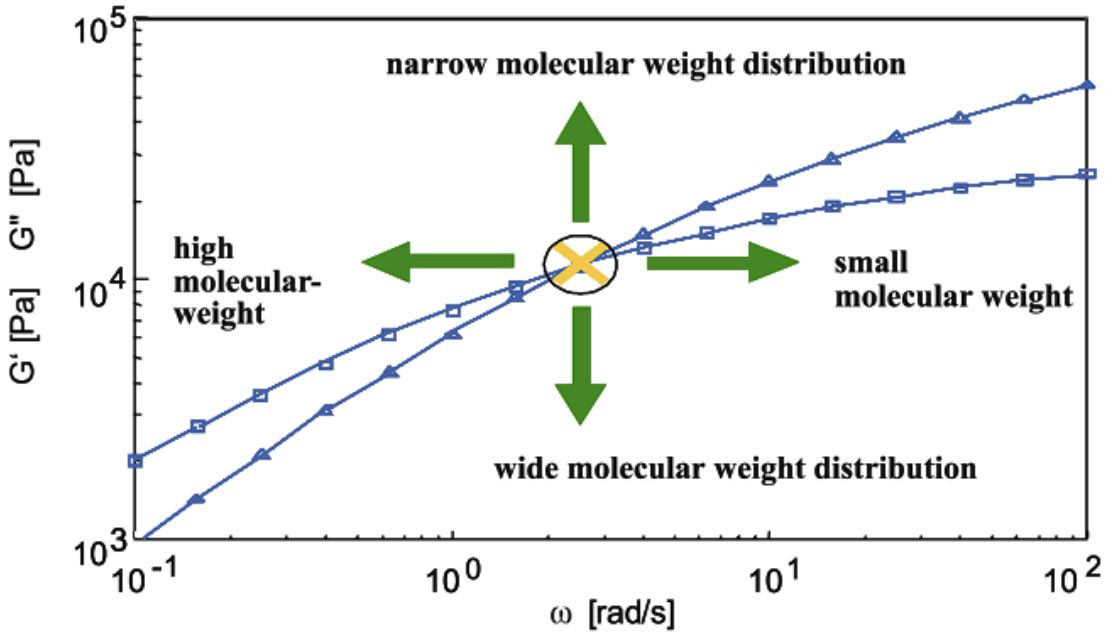

Figure 7. Effect of MW and MWD on crossover point location from ref [43]. Copyright 2006 Springer

The tabulated crossover points in Table 4 are an average of three SAOS measurements. There is a direct correlation between the MFI of the PP grade and the crossover frequency value as expected. As the MFI increases, the crossover frequency increases. For instance, PP1, with a MFI of 3.6 g/10min, exhibits the lowest crossover frequency at 18.3 rad/s, while PP3, with an MFI of 20 g/10min, shows the highest at 111 rad/s. Consequently, the printability and mechanical properties of the three different grades are expected to vary due to differences in their rheological and flow behavior. Such findings highlight the importance of considering the additive packages added by the manufacturer and PP architecture in selecting a PP grade for FFF.

Table 4. Crossover values from SAOS measurements for neat PP

Material	Crossover Frequency (rad/s)	Crossover Modulus (kPa)	MFI (g/10min)
PP1	18.3 ± 0.0	27.2 ± 0.1	3.6
PP2	40.2 ± 0.6	20.7 ± 0.5	12
PP3	111 ± 2.4	27.7 ± 0.4	20

4.3.2 Effect of HR on the Low Frequency Crossover Points of Blends

With the incorporation of HR to formulate PP blends, DSC studies have shown a reduction in the crystallinity of PP. Crystallites in semicrystalline polymers act as physical crosslinks that strengthen the polymer and result in the polymer resisting flow. As HR reduces the crystallinity of PP, less crystallites are formed resulting in a reduction in the modulus of the polymer and shortening the time scale the polymer needs to start to flow. Figure 8 show how HR affects the rheological properties of the material.

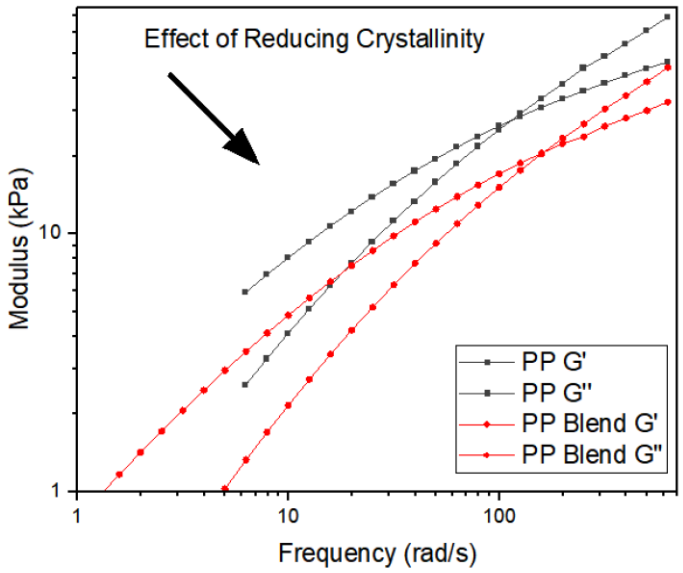

Figure 8. SAOS measurements at 180 °C showing the effect of HR incorporation with PP on the rheological properties of the blend

Table 5 tabulates the crossover points from the average of three SAOS measurements. We observe a shift in the crossover points towards higher frequency values and lower modulus values, supporting our claims that HR additives disrupt the ordered molecular structure of neat PP. This disruption allows the polymer chains in the blends to flow more readily by reducing the number of entanglements, due to the addition of foreign materials to PP. As expected, with the reduction in the ordered structure of PP, the crossover modulus decreases. We do not observe a direct correlation between the shift in the crossover point and the neat PP grade. The crossover frequency for the blends increased by 23.0%, 96.3%, and 45.9% for PP1B, PP2B, and PP3B, respectively, compared to their neat counterparts. Conversely, the crossover modulus decreased by 30.5%, 24.5%, and 24.8% for PP1B, PP2B, and PP3B, respectively. The difficulty in isolating the degree of shift for each PP grade is compounded by variations in the additive packages and molecular architecture employed by the manufacturer. An important observation is that the good mixing and

formulation of the blends are evident from the low standard deviation in the crossover values of all three blends, as shown in Table 5.

Table 5. Crossover values from SAOS measurements for blends

Material	Crossover Frequency (rad/s)	Crossover Modulus (kPa)
PP1B	22.5 ± 0.2	18.9 ± 0.2
PP2B	78.9 ± 0.9	15.7 ± 0.2
PP3B	162.0 ± 0.6	21 ± 0.3

4.3.3 Investigation of Miscibility of HR with PP

Before proceeding with printing of blends, the miscibility of HR with the different PP grades needs to be studied to ensure consistent printing results. Rheological measurements can aid this analysis by analyzing Cole-Cole plots. Using the moduli values plot in the previous figures, Equation (2) [12] can be used to compute the imaginary viscosity component (η") and the real viscosity component (η') where ω is the angular frequency (rad/s).

$$\eta'^2 + \eta''^2 = \left(\frac{G'}{\omega}\right)^2 + \left(\frac{G''}{\omega}\right)^2 \quad (2)$$

Figure 9 shows that the Cole-Cole plots result in a semi-arch profile for all the three blends, indicating good miscibility and formation of a homogenous blend [12].

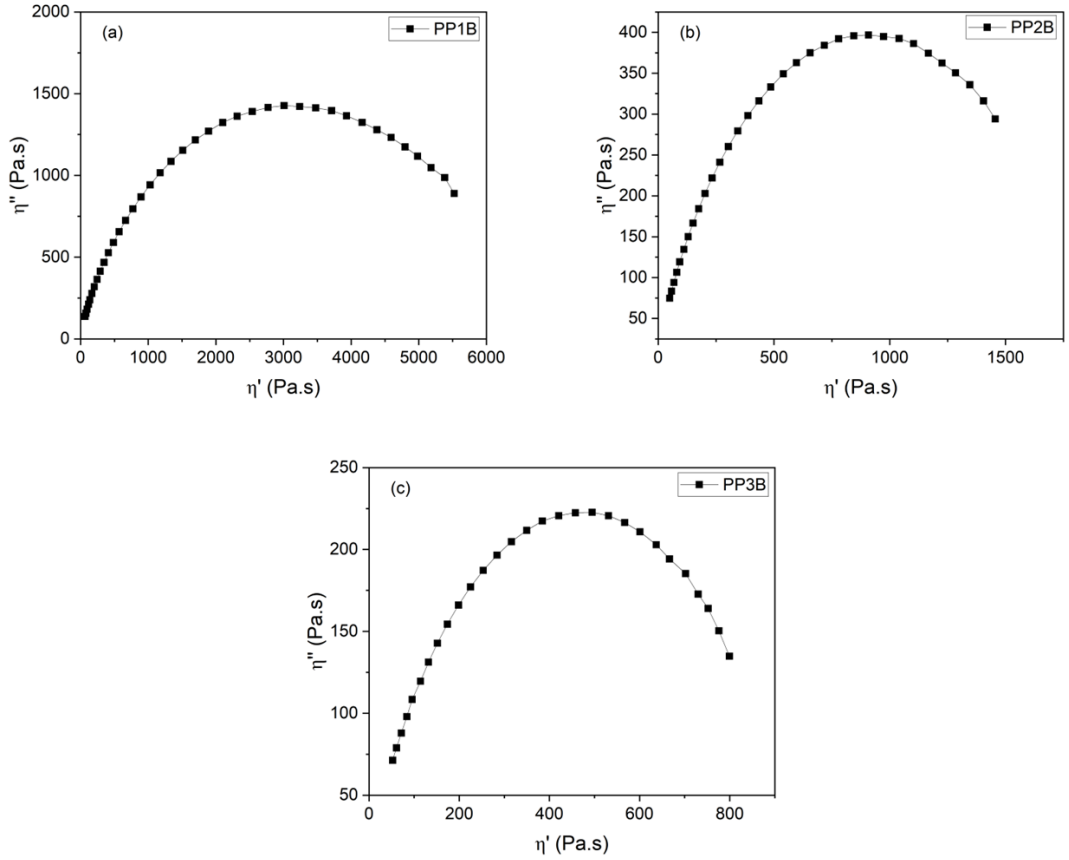

Figure 9. Cole-Cole plots showing the variation of η'' versus η' calculated from SAOS measurements at 180 °C for (a) PP1B, (b) PP2B, and (c) PP3B

4.3.4 Viscosity of Blends at MEAM Extrusion Temperature

The rheological behavior of polymers at temperatures relevant to MEAM act as an important factor in determining their rate dependent viscous response [7]. The flow behavior of polymers at different shear rates will be indicative of their printability. Figure 10 shows the variation of complex viscosity with frequency when subjected to a constant strain of 0.5 % at 200 °C. All three blends exhibit a shear thinning behavior which is desirable in MEAM. At low shear rates, the viscosity approaches a plateau resulting in the ability of the blends to set. On the other hand, at higher shear rates, the observed viscosity drop of the blends favor flowing as during extrusion. We can also see a direct correlation between the MFI of the PP grade and the shear

thinning profile. The low MFI of PP1 results in PP1B having a higher viscosity and an earlier onset of shear thinning while the opposite is true for the highest MFI PP3. The onset of shear thinning for PP1B is beyond the frequency range of the experiment. However, for PP2B and PP3B, the onset of shear thinning is around ~10 rad/s and ~40 rad/s, respectively.

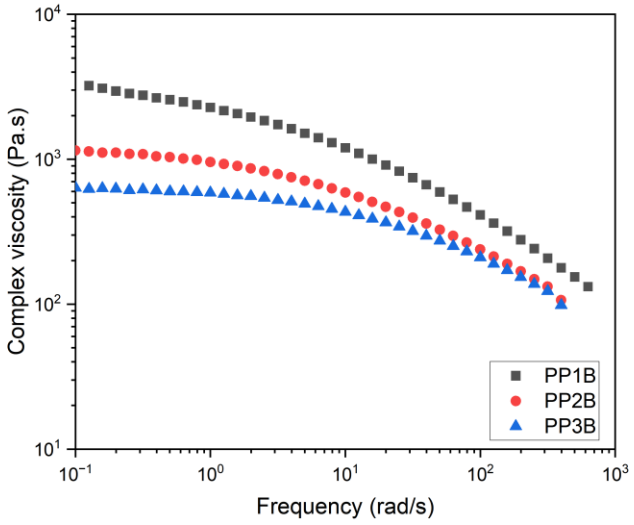

Figure 10. Complex viscosity versus frequency from SAOS measurements at 200 °C for the three blends

4.4 Mechanical and Structural Analysis Neat PP and Blend Parts

4.4.1 Mechanical Properties of Injection Molded Neat PP Grades

In order to assess the properties of the printed blends, tensile tests were performed on the neat injection molded PP grades, to establish a benchmark to compare the mechanical properties of neat PP to the mechanical properties of the printed blends. Figure 11 shows the tensile properties of the injection molded PP grades with an applied strain of 10 mm/s. There are substantial similarities between the mechanical properties of the PP grades. For instance, we see that the PP grades exhibit similar yield stress values around ~40 MPa. In addition, the elongation at break on

average is statistically similar. PP1 exhibits an elongation at break value of 660.5 %, while PP2 and PP3 show an elongation at break of 647.9 % and 632.1 %, respectively. By performing ANOVA analysis on the elongation at break data, the calculated P-value is 0.93 (> 0.05) indicating similarities between the grades. However, the standard deviation in the elongation at break results is noticeably increasing and is correlating positively with the increase in MFI of the PP grade as shown in Table 6. From the rheological data, we know that PP3 polymer chains show the shortest τ_{rep} which possibly resulted in more variability in the elongation at break results.

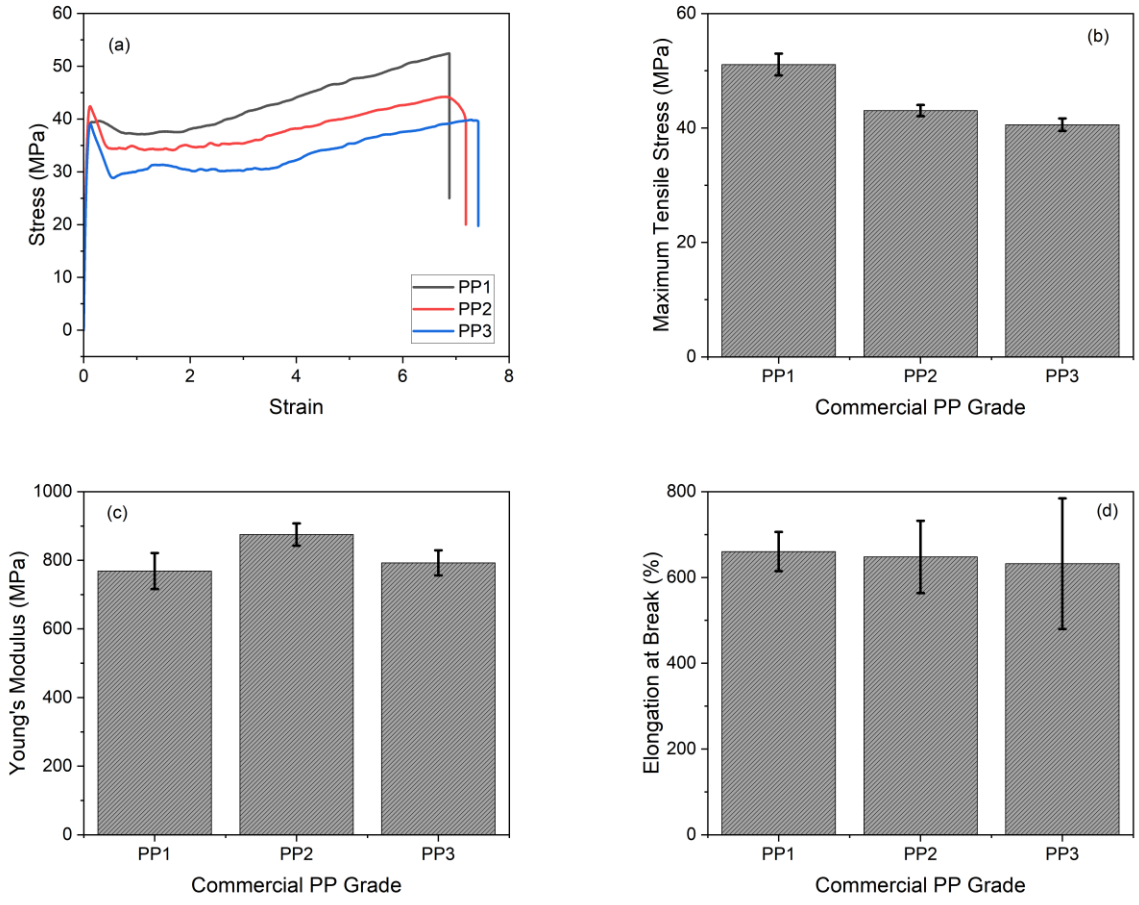

Figure 11. (a) Tensile curves for injection molded neat PP grades, (b) maximum tensile strength of injection molded neat PP grades, (c) Young's modulus of injection molded neat PP grades, (d) elongation at break of injection molded neat PP grades

On the other hand, we do not see a correlation between the Young's modulus value and the PP grade. The ANOVA analysis shows that the P-value for Young's modulus data is 0.01 (<0.05). Thus, indicating that the results are statistically different. Those differences will most likely be a result of the additive packages incorporated by the manufacture to the PP grades. A clear trend is observed when looking at the tensile strength of the PP grades, we see that the lower the MFI, the higher the maximum tensile strength. PP1 exhibits a maximum tensile strength value of 51.1 MPa while PP2 and PP3 have maximum tensile strength values of 43.1 and 40.6 MPa, respectively. A likely explanation is that PP1 exhibits more entanglements compared to the other two grades and so the mechanical strength is higher. This agrees well with the rheological discussed earlier. Table 6 tabulates the tensile properties of the injection molded neat PP grades.

Table 6. Tensile properties of injection molded neat PP grades

Material	Maximum tensile strength (MPa)	Elongation at break (%)	Young's modulus (MPa)
PP1	51.1 ± 1.9	660.4 ± 45.6	768.6 ±52.6
PP2	43.1 ± 1.0	647.9 ± 84.2	875.0 ± 32.4
PP3	40.6 ± 1.1	632.1 ± 152.3	792.8 ± 36.5

4.4.2 Printability of Neat PP

As generally accepted in the literature, PP printed parts show extreme warpage. An illustration of this is shown in the images in Figure 12 below for the case of PP2. By printing thin-walled structure of neat PP grades, we see extreme deformation and warpage. In addition, the interlayer adhesion between the deposited layers is extremely weak due to the fast crystallization kinetics.

Figure 12. Structural deformation and warpage in a thin-walled PP2 structure. Left: top view, right: side view

As a result of this, only the blends are used to print tensile bars. The mechanical properties of the printed blends are compared directly with the injection molded neat PP properties.

4.4.3 Effect of PP Grade and print orientation on Mechanical Properties of Printed Blends

By analyzing the mechanical properties of the printed blends, a better understanding of the effect of the PP grade can be established. Furthermore, by printing samples at either 0° or 90° raster angles, the print orientation can be studied to investigate printing anisotropy and interlayer adhesion. Das et. al [16] previously reported an improvement in the ultimate tensile strength of printed PP when incorporated with HR at 80:20 PP:HR wt%. As such, only this composition is printed in this study. Figure 13 shows the tensile tests data of the blends with a constant applied strain rate of 10 mm/s. We observe that the printed parts exhibit a brittle fracture. This is most likely a result of the blends exhibiting a two phase morphology with a PP rich domain and a HR rich domain as previously reported [16].

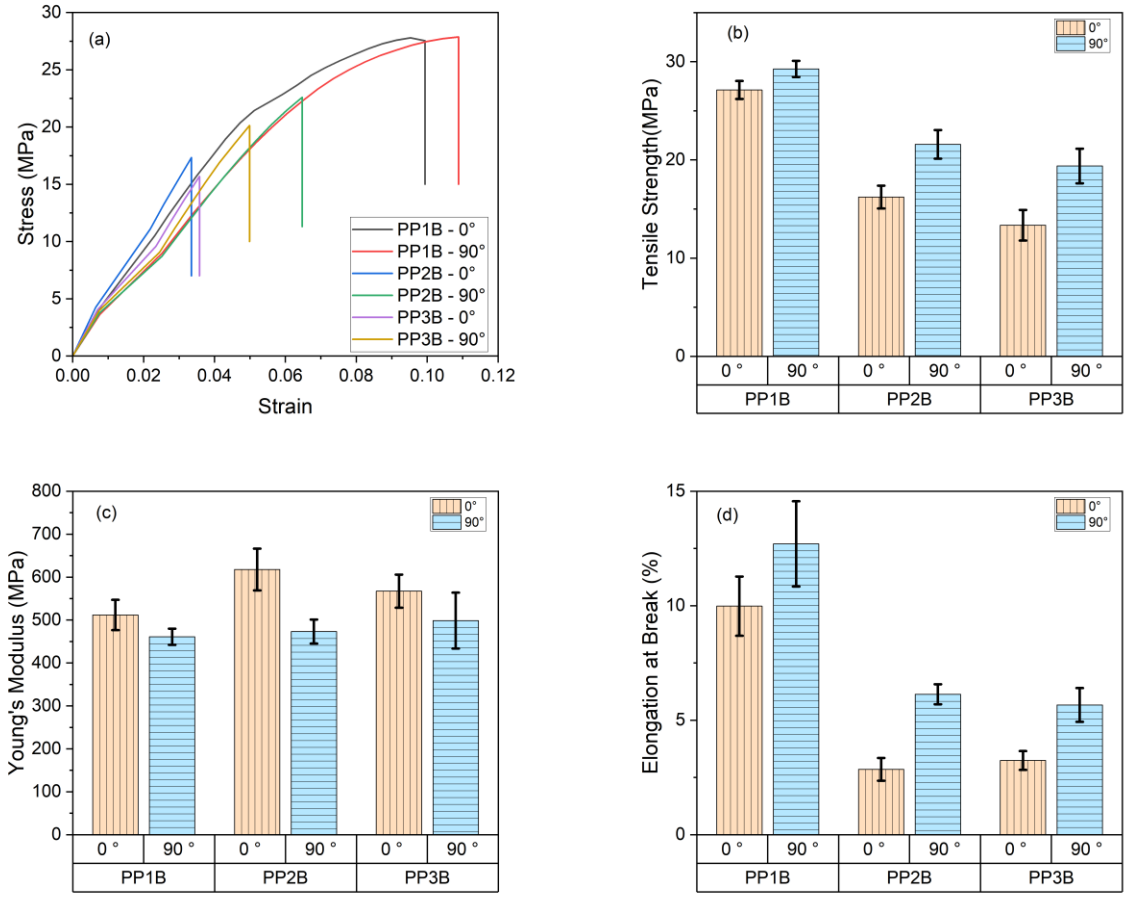

Figure 13. (a) stress versus strain curves for printed blend parts, (b) maximum tensile strength of printed blend parts, (c) Young's modulus of printed blend parts, (d) elongation at break of printed blend parts

In our analysis of maximum tensile strength, we find a direct correlation with the results for the injection molded PP grades presented in Table 6. PP1 consistently shows the highest tensile strength across all print orientations, while PP3 has the lowest, likely due to inherent differences in the mechanical properties of the neat PP grades. Surprisingly, the mechanical results related to print orientation contradicted expectations. It is generally understood that parts printed at 0° are stronger because the failure is due to material failure along fully entangled roads, whereas parts printed at 90° are weaker due to failures at the interlayer welds from incomplete re-entanglement

before crystallization [44]. However, the trend observed in Figure 13 suggests that the print path and part size significantly influence mechanical properties. Ai et al. [45] recently found that the print path and part geometry play an important role in the resulting mechanical properties of the prints. They observed that a shorter interlayer time between adjacent roads, which occurs in 90° prints, results in a smaller temperature gradient during deposition. This smaller gradient enhances interlayer adhesion, thereby strengthening the parts. Consequently, the 90° prints exhibited higher tensile strengths of 29.3 MPa, 21.6 MPa, and 19.4 MPa for PP1B, PP2B, and PP3B, respectively, compared to the 0° prints, which showed tensile strengths of 27.1 MPa, 16.2 MPa, and 13.3 MPa for the same grades. These results highlight the complex interplay between print orientation and part geometry in determining the mechanical properties of printed parts.

However, we observed that the degree of improvement in interlayer adhesion varies depending on the PP grade in the blend. PP1B showed the least improvement, indicating that its interlayer adhesion does not enhance to the same extent as blends with higher MFIs and thus higher crossover frequencies. In contrast, the 90° prints of PP3B demonstrated the most significant improvement in mechanical strength compared to the 0° prints, owing to a greater extent of interlayer adhesion. For PP1B, the print orientation does not drastically affect the mechanical strength; however, an increase in the crossover frequency correlates with greater anisotropy in print orientation. Specifically, the percentage difference in tensile strength due to print orientation is approximately 8% for PP1B, while it is about 33% for PP2B and 46% for PP3B. These variations are shown in Table 7, which tabulates the tensile properties of the blends.

Table 7. Tensile properties of printed blends

Material	Raster angle (°)	Ultimate tensile strength (MPa)	Elongation at break (%)	Young's modulus (MPa)
PP1B	0	27.1 ± 0.9	10.0 ± 1.3	551.8 ± 35.3
PP1B	90	29.3 ± 0.8	12.7 ± 1.9	461.0 ± 18.9
PP2B	0	16.2 ± 1.2	2.9 ± 0.5	617.6 ± 48.7
PP2B	90	21.6 ± 1.5	6.1 ± 0.4	473.2 ± 28.0
PP3B	0	13.3 ± 1.6	3.2 ± 0.4	567.2 ± 38.6
PP3B	90	19.4 ± 1.8	5.7 ± 0.7	498.7 ± 65.0

As for the Young's modulus, for 0° prints, the values follow a similar trend to that of the injection molded neat PP grades , albeit with lower values. Specifically, Young's modulus for 0° prints is 551.8 MPa for PP1B, 617.6 MPa for PP2B, and 567.2 MPa for PP3B. In contrast, for 90° prints, the values are statistically similar, with a P-value of 0.48 (> 0.05), indicating no significant difference. However, a slight increase in Young's modulus is observed from PP1B (461.1 MPa) to PP3B (498.7 MPa). This increase is likely due to the effect of improved interlayer adhesion. This trend highlights the influence of print orientation on the mechanical properties of the printed blends. Compared to the 0° prints, Young's modulus values for the 90° prints are generally lower. This could be attributed to the fact that in 0° prints, part failure often results from the brittleness of the blend, whereas in 90° prints, the higher strain at failure may be due to failures at the interlayer welds, which are likely dominated by the presence of amorphous HR.

4.4.4 Effect of PP Grade on Warpage of Printed Blends

While warpage has been shown to be minimized by the incorporation of hydrocarbon resins [16], the extent of this reduction is dependent on the PP grade used. Figure 14 shows the average warpage of five prints as a function of blend type and print orientation. PP1B showed the highest warpage of 1.3 mm for the 0° prints while PP3B showed the least warpage of 0.88 mm for the 90° prints. Similar to our previous arguments, the blends with higher crossover frequency will have better interlayer adhesion. As a result, the volume shrinkage, and residual stresses that result with the use of semicrystalline polymers can be reduced with better interlayer adhesion. Likewise, the 90° shows slightly less warpage compared to their 0° because of the reduced interlayer time between the deposited roads.

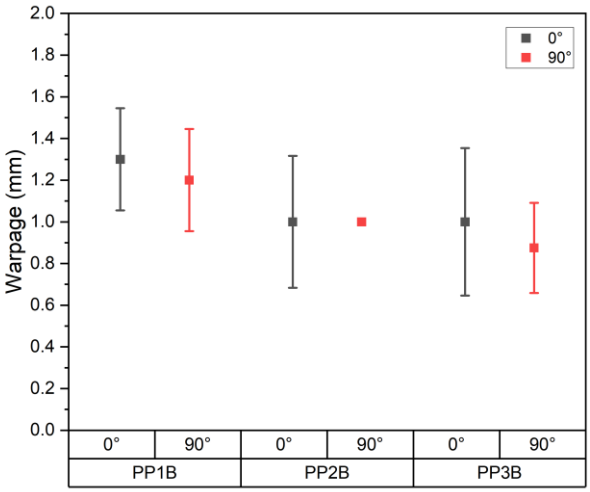

Figure 14. Print parts warpage as a function of blend type and print orientation

5 CONCLUSIONS

The crossover point of G' and G'', as measured using SAOS, serves as an indicator for evaluating the impact of additive packages and molecular architecture of commercial PP grades of similar MW and MWD in FFF. A relatively higher crossover frequency will correlate with improved interlayer adhesion and reduced warpage in printed structures. However, this improvement is accompanied by a tradeoff, resulting in inferior tensile strength and an increased degree of print orientation anisotropy. This relationship was demonstrated by comparing the rheology and printability of three commercial PP grades. PP3B, which has the highest crossover frequency, demonstrated the highest degree of interlayer adhesion but also exhibited a high degree of print anisotropy and relatively weaker tensile strength prints. In contrast, PP1B, with the lowest crossover frequency, displayed the highest tensile strength and minimal print anisotropy, despite its relatively lower extent of interlayer adhesion. Therefore, the selection of PP grades for FFF applications should consider not only MW and MWD but also the differences in additive packages and polymer architecture that exist across commercially sourced polymers, regardless of the manufacturer. These factors are typically difficult to isolate, and the rheological methods explored in this study could potentially be expanded to encompass other PP materials, even those with little known specifications.

Furthermore, the addition of HR to PP has been shown to impact crystallizability, crystallinity, and melting properties, aiding in reducing warpage and structural deformations that neat PP prints usually experience. However, the specific effects of HR on the thermal properties of different PP grades require further understanding. Additionally, the inclusion of HR influences the rheological properties of the blends, resulting in a shift in the crossover points towards shorter relaxation times, which further enhances interlayer adhesion.

6 FUTURE WORK

Future work will focus on a more detailed analysis of the crystallization kinetics by utilizing Flash DSC analysis to achieve cooling rates representative of the FFF process. This will provide better understanding of the effect of HR on the crystallization kinetics of PP and the underlying impact on printability. Furthermore, the impact of HR on morphology needs to be better understood. The extent of the shift in the peak crystallization temperatures was different for different grades suggesting differences in the morphological changes that HR resulted in those grades. This can be studied with the aid of microscopy techniques such as Scanning Electron Microscope (SEM).

Further enhancement to the mechanical properties of the printed blends can be achieved via printing process optimization. Smaller layer heights may improve interlayer adhesion, thereby enhancing mechanical properties. Furthermore, adjustments to printing speed and print bed temperature should be explored to optimize printability and mechanical properties. A current limitation is the upper extrusion temperature cap of 200 °C due to the thermal stability of HR. Investigating other hydrocarbon resins with higher thermal stability might allow for increased extrusion temperatures, which could further explore the effect of extrusion temperature on PP blends.

Additionally, the applicability of rheological techniques explored in this study in comparing the printability of PP grades with varying degrees of crystallinity needs to be assessed. This evaluation will determine if these techniques are adequate for understanding the printability of PP grades with a broad range of properties.

Finally, due to significant warpage, the mechanical properties of printed neat PP were not investigated in this study. Future efforts should include methods to characterize these properties to facilitate a direct comparison with printed blends, thus providing a fuller understanding of the effects of HR on enhancing printability.

7 REFERENCES

1. Ford, S. and M. Despeisse, *Additive manufacturing and sustainability: an exploratory study of the advantages and challenges.* Journal of Cleaner Production, 2016. **137**: p. 1573-1587.
2. Gao, W., et al., *The status, challenges, and future of additive manufacturing in engineering.* Computer-Aided Design, 2015. **69**: p. 65-89.
3. Ngo, T.D., et al., *Additive manufacturing (3D printing): A review of materials, methods, applications and challenges.* Composites Part B: Engineering, 2018. **143**: p. 172-196.
4. Dey, A., I.N. Roan Eagle, and N. Yodo, *A Review on Filament Materials for Fused Filament Fabrication.* Journal of Manufacturing and Materials Processing, 2021. **5**(3): p. 69.
5. N. Turner, B., R. Strong, and S. A. Gold, *A review of melt extrusion additive manufacturing processes: I. Process design and modeling.* Rapid Prototyping Journal, 2014. **20**(3): p. 192-204.
6. Bertolino, M., et al., *Designing 3D printable polypropylene: Material and process optimisation through rheology.* Additive Manufacturing, 2021. **40**: p. 101944.
7. Das, A., et al., *Rheology, crystallization, and process conditions: The effect on interlayer properties in three-dimensional printing.* Physics of Fluids, 2022. **34**(12).
8. Gao, X., et al., *Fused filament fabrication of polymer materials: A review of interlayer bond.* Additive Manufacturing, 2021. **37**: p. 101658.
9. Bachhar, N., et al., *3D printing of semicrystalline polypropylene: towards eliminating warpage of printed objects.* Bulletin of Materials Science, 2020. **43**(1): p. 171.
10. Fico, D., et al., *A Review of Polymer-Based Materials for Fused Filament Fabrication (FFF): Focus on Sustainability and Recycled Materials.* Polymers, 2022. **14**(3): p. 465.
11. Spoerk, M., C. Holzer, and J. Gonzalez-Gutierrez, *Material extrusion-based additive manufacturing of polypropylene: A review on how to improve dimensional inaccuracy and warpage.* Journal of Applied Polymer Science, 2020. **137**(12): p. 48545.
12. Das, A., N. Shanmugham, and M.J. Bortner, *Customized blends of polypropylene for extrusion based additive manufacturing.* Journal of Vinyl and Additive Technology, 2023. **29**(4): p. 649-661.
13. Peng, X., et al., *Shape memory effect of three-dimensional printed products based on polypropylene/nylon 6 alloy.* Journal of Materials Science, 2019. **54**(12): p. 9235-9246.
14. Yi, N., et al., *Slow and fast crystallising poly aryl ether ketones (PAEKs) in 3D printing: Crystallisation kinetics, morphology, and mechanical properties.* Additive Manufacturing, 2021. **39**.
15. Spoerk, M., et al. *Optimisation of the Adhesion of Polypropylene-Based Materials during Extrusion-Based Additive Manufacturing*. Polymers, 2018. **10**, DOI: 10.3390/polym10050490.
16. Das, A., et al., *Material Extrusion-Based Additive Manufacturing with Blends of Polypropylene and Hydrocarbon Resins.* ACS Applied Polymer Materials, 2020. **2**(2): p. 911-921.
17. Wohlers, T., et al., *History of additive manufacturing.* 2016.
18. Chua, C.K. and K.F. Leong, *3d Printing And Additive Manufacturing: Principles And Applications (With Companion Media Pack) - Fourth Edition Of Rapid Prototyping*. 2014: World Scientific Publishing Company.

19. Tofail, S.A., et al., *Additive manufacturing: scientific and technological challenges, market uptake and opportunities.* Materials today, 2018. **21**(1): p. 22-37.
20. Herzog, D., et al., *Additive manufacturing of metals.* Acta Materialia, 2016. **117**: p. 371-392.
21. Deckers, J., J. Vleugels, and J.-P. Kruth, *Additive manufacturing of ceramics: A review.* Journal of Ceramic Science and Technology, 2014. **5**(4): p. 245-260.
22. González-Henríquez, C.M., M.A. Sarabia-Vallejos, and J. Rodriguez-Hernandez, *Polymers for additive manufacturing and 4D-printing: Materials, methodologies, and biomedical applications.* Progress in Polymer Science, 2019. **94**: p. 57-116.
23. Das, A., et al., *Importance of Polymer Rheology on Material Extrusion Additive Manufacturing: Correlating Process Physics to Print Properties.* ACS Applied Polymer Materials, 2021. **3**(3): p. 1218-1249.
24. Qattawi, A., B. Alrawi, and A. Guzman, *Experimental optimization of fused deposition modelling processing parameters: a design-for-manufacturing approach.* Procedia Manufacturing, 2017. **10**: p. 791-803.
25. Turner, B.N. and S.A. Gold, *A review of melt extrusion additive manufacturing processes: II. Materials, dimensional accuracy, and surface roughness.* Rapid Prototyping Journal, 2015. **21**(3): p. 250-261.
26. Valkenaers, H., et al. *A novel approach to additive manufacturing: screw extrusion 3D-printing*. in *Proceedings of the 10th international conference on multi-material micro manufacture*. 2013. Research Publishing; Singapore.
27. Boiko, Y.M., et al., *Healing of interfaces of amorphous and semi-crystalline poly(ethylene terephthalate) in the vicinity of the glass transition temperature.* Polymer, 2001. **42**(21): p. 8695-8702.
28. Xue, Y.Q., et al., *Welding Behavior of Semicrystalline Polymers. 2. Effect of Cocrystallization on Autoadhesion.* Macromolecules, 2000. **33**(19): p. 7084-7087.
29. Karger-Kocsis, J. and T. Bárány, *Polypropylene handbook.* Switzerland: Springer Nature, 2019.
30. Maddah, H.A., *Polypropylene as a promising plastic: A review.* Am. J. Polym. Sci, 2016. **6**(1): p. 1-11.
31. Jagenteufel, R., et al., *Rheology of high melt strength polypropylene for additive manufacturing.* Advanced Materials Letters, 2017. **8**(6): p. 712-716.
32. Wang, L. and D.J. Gardner, *Effect of fused layer modeling (FLM) processing parameters on impact strength of cellular polypropylene.* Polymer, 2017. **113**: p. 74-80.
33. Hämäläinen, J.P., *Semi-crystalline polyolefins in fused deposition modeling*. 2017.
34. Spoerk, M., et al., *Optimization of mechanical properties of glass-spheres-filled polypropylene composites for extrusion-based additive manufacturing.* Polymer Composites, 2019. **40**(2): p. 638-651.
35. Silvestre, C., et al., *Crystallization of isotactic polypropylene/natural terpene resins blends.* Polymer, 1999. **40**(18): p. 5119-5128.
36. Cimmino, S., et al., *Blends of isotactic polypropylene and natural terpene resins. I. Phase structure, thermal, and dynamic-mechanical properties.* Journal of Polymer Science Part B: Polymer Physics, 1999. **37**(9): p. 867-878.
37. Baouch, Z., et al., *Polypropylene for material extrusion: Evidence that flow-enhanced crystallization restricts welding.* Additive Manufacturing, 2024. **83**: p. 104063.

38. Bagheriasl, D., et al., *Properties of polypropylene and polypropylene/poly (ethylene-co-vinyl alcohol) blend/CNC nanocomposites.* Composites Science and Technology, 2015. **117**: p. 357-363.
39. An, Y., et al., *Effect of different nucleating agent on crystallization kinetics and morphology of polypropylene.* e-Polymers, 2019. **19**(1): p. 32-39.
40. Kang, J., et al., *Hydrogenated petroleum resin effect on the crystallization of isotactic polypropylene.* Journal of Applied Polymer Science, 2013. **130**(1): p. 25-38.
41. Rubinstein, M. and R.H. Colby, *Polymer physics*. 2003: Oxford university press.
42. Oveby, C., *Characterisation of molecular structure of polymers by rheological methods.* ANNUAL TRANSACTIONS-NORDIC RHEOLOGY SOCIETY, 1998. **6**: p. 129-132.
43. Brummer, R., *Rheology essentials of cosmetic and food emulsions.* 2006.
44. Çakan, B.G., *Effects of raster angle on tensile and surface roughness properties of various FDM filaments.* Journal of Mechanical Science and Technology, 2021. **35**(8): p. 3347-3353.
45. Ai, J.-R. and B.D. Vogt, *Size and print path effects on mechanical properties of material extrusion 3D printed plastics.* Progress in Additive Manufacturing, 2022. **7**(5): p. 1009-1021.